the collisional recombination process of Ar^+. The same results were obtained previously for the helium and neon atomic ions.[10-12]

For argon concentrations of 1 and 5%, Ar_2^+ ions were also observed, although, for the experimental conditions, the Ar^+ ions were the majority ions. These studies led to the verification, for the first time by simultaneous light emission and ion-density measurements, of the dissociative recombination of Ar_2^+ with electrons. The importance of this recombination process has previously been established by line-broadening studies[4] as well as by the large recombination coefficient measured for the Ar_2^+ ion.[1,3] The present studies strongly indicate that the dissociative recombination process populates directly only the $2p$ and $3p$ energy levels.

ACKNOWLEDGMENT

The discussions with other members of the study group on collision processes have been very helpful.

*Work supported by the Air Force Research Laboratories, Office of Aerospace Research (Contract No. AF 19(628)-4794) and National Science Foundation (Grant No. GK-10395).

[1]M. A. Biondi, Phys. Rev. 83, 1078 (1951).

[2]H. J. Oskam, Philips Res. Rept. 13, 335 (1958).

[3]A. Redfield and R. B. Holt, Phys. Rev. 82, 874 (1951).

[4]L. Frommhold and M. A. Biondi, Phys. Rev. 185, 244 (1969).

[5]G. F. Sauter, R. A. Gerber, and H. J. Oskam, Rev. Sci. Instr. 37, 572 (1966).

[6]D. Alpert, J. Appl. Phys. 24, 860 (1953).

[7]R. Riesz and G. H. Dieke, J. Appl. Phys. 25, 196 (1954).

[8]T. Holstein, Phys. Rev. 100, 1230 (1955).

[9]M. A. Biondi and L. M. Chanin, Phys. Rev. 122, 843 (1961).

[10]R. A. Gerber, G. F. Sauter, and H. J. Oskam, Physica 32, 2173 (1966).

[11]G. F. Sauter, R. A. Gerber, and H. J. Oskam, Physica 32, 1921 (1966).

[12]G. E. Veatch and H. J. Oskam (unpublished).

[13]A. V. Phelps, Proceedings of the Third International Conference on Inization Phenomena in Gases, Venice, 1957 (unpublished), p. 818.

[14]Principal quantum number of the energy levels studied is believed to be sufficiently small such that the emission intensity is proportional to the recombination rate.

[15]D. K. Bohme, D. B. Dunkin, F. C. Fehsenfeld, and E. E. Ferguson, J. Chem. Phys. 51, 863 (1969).

[16]K. B. McAfee, D. Sipler, and D. Edelson, Phys. Rev. 160, 160 (1967).

[17]Paschen notation is used for the levels.

PHYSICAL REVIEW A VOLUME 1, NUMBER 5 MAY 1970

Excitation of Ionized Helium States in a Cooled Hollow-Cathode Discharge*

H. G. Berry† and F. L. Roesler

Department of Physics, University of Wisconsin, Madison, Wisconsin 53706

(Received 3 April 1969; revised manuscript received 26 November 1969)

A high-resolution study of the He II λ4686 Å ($n=3-4$) line complex emitted from a cooled hollow cathode has been made using a double-etalon spectrometer with photoelectric detection. Computer analysis of the digitally recorded spectra of this line yields fine-structure and isotope-shift measurements for the isotopes ^3He and ^4He which agree with quantum electrodynamic theory to within ± 0.0005 cm^{-1} for the best measured components. The excitation and deexcitation processes for this transition, which are active in the hollow-cathode, have been analyzed. The results show that the anomalously large widths observed in ionized helium lines which have been electronically excited arise from large momentum transfers in the excitation process. Calculation of the momentum-transfer line profile in the process $He+e \rightarrow He^{+*}+e+e$ gives reasonable agreement with the observed profiles when the instrumental profile and neutral He Doppler profile are included. Measurements further confirm that the origin of the small anode-drift shift is a residual electric field within the discharge.

I. INTRODUCTION

High-resolution spectroscopic measurements of the hydrogenlike lines of He^+ have previously been undertaken primarily to improve the measurement of the relative component positions for comparison with the quantum electrodynamical predictions.[1–4] In every instance, however, anomalies have been revealed in some of the measured parameters: positions, widths, and relative intensities of the spectral components. These anomalies can be related to the atomic processes occurring within the hollow-cathode discharge, and thus can reveal information about the discharge mechanisms. We study here the anomalies in the measurements of the $He^+ n = 4 \rightarrow 3$ line complex at λ4686 Å to improve our understanding of the hollow-cathode discharge. The level structure for this transition is shown in Fig. 1.

II. EXPERIMENT

Figure 2 shows the experimental arrangement. Up to three hollow cathodes could be cooled in liquid helium or in liquid nitrogen, and the light emitted from one was directed into one of the spectrometers. The cathodes were of the double-anode type, and measurements were made using each one alternately. This was necessary to average out small relative shifts in the fine-structure components due to an axially directed electric field within the discharge (see Sec. VII). Electrodes of copper, kovar, and aluminum were used; those of aluminum produced the coolest discharges. Glass-to-metal seals for copper and aluminum electrodes, which could withstand repeated cooling in liquid helium, were obtained by machining the metal to a thin (~4 mil) lip and sealing it to the glass with Bondmaster M640 epoxy.

The emitted cathode light was analyzed by a three-etalon PEPSIOS[5] spectrometer, or by a Wisconsin-Bellevue Spectrometer (WBS) consisting of a 1-m Ebert-Fastie grating pre-monochromator coupled to two Fabry-Perot interferometers in series. Photoelectric detection in both cases was by a liquid-nitrogen-cooled 1P28 photomultiplier.

Two etalons were necessary to provide a spectral range large enough to include all the fine structure while still maintaining sufficient resolution (400 000). The third etalon in the PEPSIOS or the grating in the WBS suppressed the remaining light from a strong neutral line only 27 Å away at 4713 Å. In the hollow-cathode emission this line is about 100 times stronger than the strongest component of the HeII λ4686 Å complex. The WBS was temperature stabilized with water flowing around the etalon chambers from a large reservoir. For accurate position measurements of the fine structure, the room temperature also had to be maintained constant to ±1 °C.

In the PEPSIOS scans, the calibration fringes were produced from a Michelson interferometer operated in Hg λ5461 Å light, one arm being fixed and the other arm containing a windowed chamber which was pressure scanned with the main PEPSIOS etalon chamber. The WBS spectra were calibrated with a single long-spacer (50 mm) etalon, but illuminated with the ^{198}Hg singlet λ4047 Å or λ4358 Å. These fringes determined the wave-number scale of the spectrum, thus avoiding errors arising from nonlinearity of the scan rate.

The spectra were recorded digitally on paper tape, and simultaneously on an analog strip-chart recorder. The digital system operated from digitizing drums attached to the output drives of the two-pen recorder (the second pen recorded the wave-number calibration fringes). The two signals were recorded alternately on the paper tape at rates of up to 5 times a sec. One scan of the fine-structure complex took approximately 25 min,

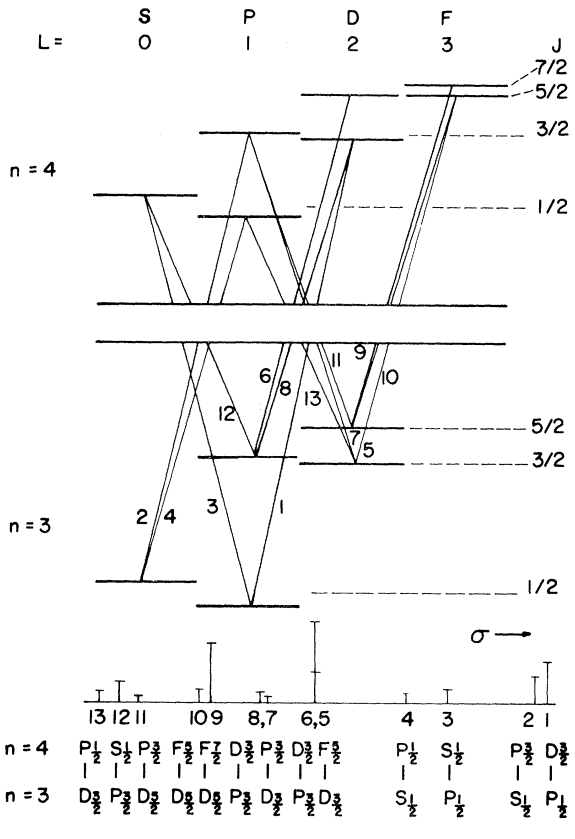

FIG. 1. Energy-level diagram for the He II λ4686 Å transition. Approximate relative positions and intensities of the 13 components are shown below the level diagram. The allowed transitions are numbered 1–13 and identified at the bottom of the figure.

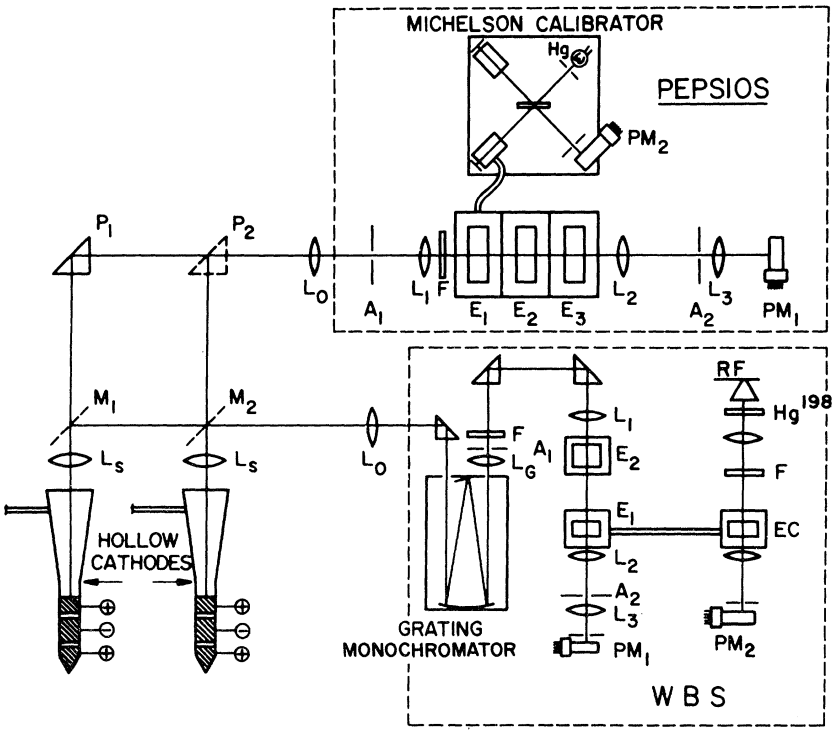

FIG. 2. Sources and spectrometers.

with 800 points being recorded over the 3-cm^{-1} scanning range.

III. REDUCTION OF DATA

The spectra were analyzed using a computer program to make a nonlinear least-squares fit of the data with a model which had as parameters the width, position, and intensity of each fine-structure component. Three different types of formulation were used. The first fitted all components to a profile selected from the violet wing of a strong component within the spectrum. The second described the profile with two parameters α and β in the form

$$I(\sigma) = h/[1 + \alpha(\sigma - \sigma_0)^2 + \beta(\sigma - \sigma_0)^4] \ ,$$

where σ_0 is the component position and h is its intensity. Other two-parameter forms were tested, but always produced a higher least-squares sum. The third technique used a functional form of the double-etalon spectrometer function. This was convoluted with a source function represented by the convolution of a square function and Lorentzian function. The half-widths of these last two functions became the two parameters for the profile. The functional form of this instrument function and its deconvolution from polyetalon spectra are treated more generally in another paper.[6] Because of a fortunate intensity distribution in the fine-structure components, shown in Figs. 3 and 4, it was possible to choose the etalon spacers ($l_1 = 7.979$ mm; $l_2 = 1.773$ mm) such that subsidiary ghost intensities were negligible in separated isotope scans. This may be deduced by comparing the two-etalon passband shown in Fig. 5 with Figs. 3 and 4. Only in the analysis of the isotope mixture was it necessary to include ghost lines. We found that all three fitting programs gave comparable results. For strong components, the positions typically had standard deviations of 0.0001 cm^{-1}, with intensity and halfwidth accuracy of about 1%. The weaker, blended components were less accurately known: ± 0.001 to 0.005 cm^{-1} in position and 5 to 10% in intensity and half-width. The fine-structure positions relative to the most violet transition are given in Table I. These positions have been corrected for small variations in the calibration system which were found to produce linear errors in the wave-number scale of up to 0.3%. Hence, each spectrum had to be normalized to the best known separation: that between components 1 and 9. All other separations then agree with theory.[7]

The fine structure of the isotope ^{3}He is identical within 0.0001 cm^{-1}, but shifted relative to that of ^{4}He by the normal mass isotope shift. Table I gives the result for this isotope shift in agreement with the theoretical value of 0.9570 cm^{-1}.[7] The Lamb shifts $S(n, j)$ given in Table II are obtained from the separations in Table I, and are seen to agree with theory.[7]

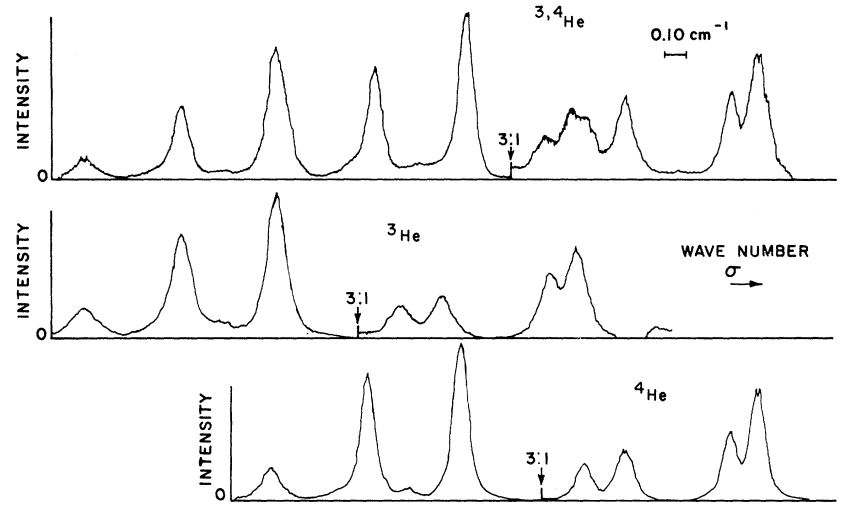

FIG. 3. He II λ4686 Å spectrum excited in a helium-cooled-aluminum hollow cathode, observed with a two-etalon spectrometer. The top scan is of an isotope mixture of ^{3}He and ^{4}He, and the second and third of ^{3}He and ^{4}He, respectively. The three scans are positioned to indicate the isotope shift $\Delta = 0.957$ cm^{-1}. Note the intensity-scale change of 3:1 in each scan; the components on the left have been reduced by a factor of 3.

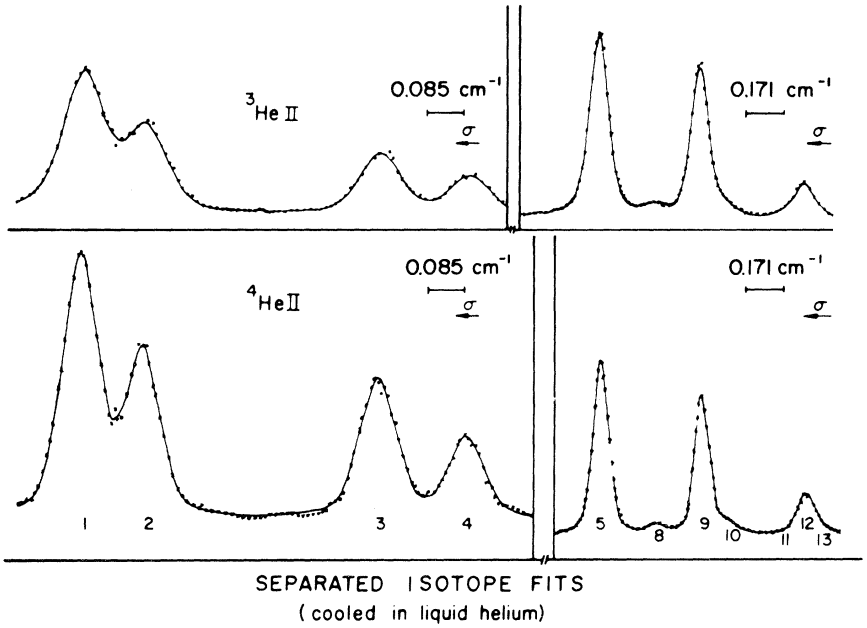

FIG. 4. Computed fits to the fine structure of the separated isotopes ^{3}He (upper) and ^{4}He for the transition at λ4686 Å ($n = 4 \rightarrow 3$). The crosses represent data points and the full line is the functional fit. The wave-number scale for components 1–4 is expanded by a factor of 2 and the intensity scale by a factor of 3 compared with the scales for components 5–13.

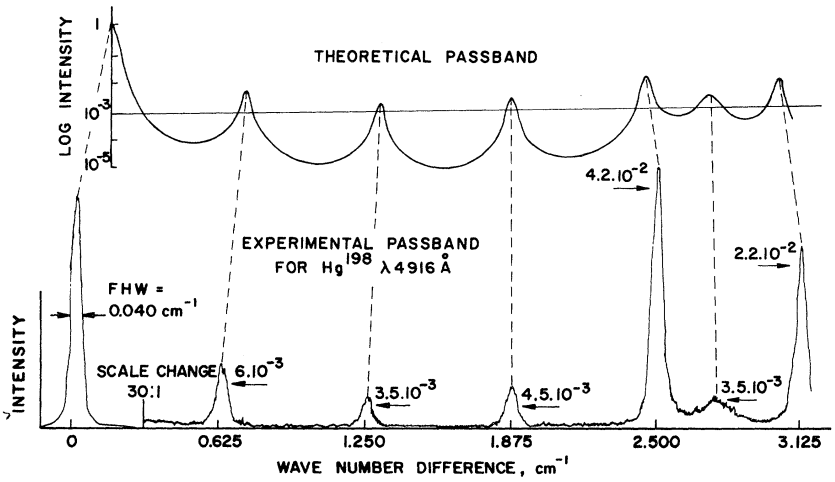

FIG. 5. Comparison of the theoretical and experimental two-etalon passbands. A narrow ^{198}Hg line at λ4916 Å was used as a source for the system. Quantitative agreement was obtained when using the known plate flatness, plate reflectance, and entrance-aperture diameter in the theoretical instrumental function.

TABLE I. Fine-structure relative positions for the He II $n=4\rightarrow 3$ line complex, expressed in 10^{-3} cm^{-1}.

Component	^{4}He [a]	^{3}He [a]	Theory [b]
1	0.0 ± 0.2	0.0 ± 0.2	0.0
2	137.8 ± 0.6	138.7 ± 1.0	138.2
3	675.5 ± 2.5	671.1 ± 2.5	671.8
4	871.7 ± 1.1	871.4 ± 1.5	870.4
5, 6	1490.0 ± 0.3	1490.5 ± 0.5	1489.9
7, 8	1742.2 ± 4.5	1737.3 ± 4.5	1736.0
9	1945.3 ± 0.0	1945.3 ± 0.0	1945.3
10	2064.3 ± 2.8	2057.1 ± 2.5	2057.3
11	2300. ± 45.	2337. ± 45.	2309.7
12	2407.7 ± 1.0	2407.4 ± 1.0	2407.2
13	2494. ± 35.	2440. ± 40	2463.4
Isotope shift		956.8 ± 0.3	957.0

[a] Errors are the average differences of ten or more scans, and are approximately three times the rms. deviations estimated for a single scan.

[b] Theoretical position of the blended components is the center of gravity of the blend based on statistical relative intensities.

Tables III and IV show, respectively, the results on the observed half-widths and excitation rates. The latter are derived from the observed relative intensities using the calculated mean lives[3] of the $(4, l)$ states. The intensity results of the present hollow-cathode experiment are essentially identical with those of the previous study.[4] The values in these tables are grouped according to the l value of the $n=4$ state of the components in anticipation of the discussion in Sec. V. Also included in Table IV for later reference are calculated rates for the processes to be discussed in Sec. V.

In Sec. IV, we consider first a semiquantitative description of the general features of the discharge, some of which are well known. In Sec. V, possible excitation modes of the He^{+*} $(n=4, l)$ states are considered. The relative importance of these different excitation modes in the discharge can be derived from the experimental intensities of the various spectral components, and also compared with similar excitation in a helium atomic beam.[8] In Sec. VI, we discuss the collision processes involved in the decay of the $n=4$ states, showing that the excitation mechanism must be responsible for the excessive linewidths. The component positions

TABLE II. Lamb shifts for the $n=3$ and $n=4$ levels of He^+, expressed in 10^{-3} cm^{-1}.

$S(n, j)$	^{4}He	^{3}He	Theory
$S(4, \frac{1}{2})$	57.1 ± 2.0	60.3 ± 2.0	59.0
$S(3, \frac{1}{2})$	139.1 ± 2.0	140.0 ± 1.0	139.5

TABLE III. Experimental half-widths of the observed components expressed in 10^{-3} cm^{-1}.

	Ionized helium, upper state				Neutral helium
	$4s$	$4p$	$4d$	$4f$	4713 Å
^{4}He total width	103	97	96	89	61
^{3}He total width	120	112	110	103	66
^{4}He decon. width [a]	94	87	85	76	45
^{3}He decon. width [a]	112	103	103	93	51
Ratio $\frac{3}{4}$	1.19	1.19	1.21	1.22	1.13
Atomic beam ^{4}He decon. width [a, b]	103	92	86	86	8 [c]

[a] The deconvoluted widths are derived from the total widths by deconvolution to remove instrumental broadening.

[b] From Ref. 8.

[c] This is the observed width of the 5015 Å line of He I. The triplet line 4713 Å is very weakly excited in the atomic beam and was not measured (Ref. 8).

TABLE IV. Relative excitation rates for the $n=4$ levels of He^+.

Upper state	Mean life (10^{-8} sec)	hollow cathode [a, b]	atomic beam [a, c]	R_d	R_{He^+}	$R_{He^{++}}$
4s	1.415 4	1.00	1.00	1.00 [d]	1.00 [d]	1.00 [d]
4p	0.076 87	1.60	1.09	0.43	12.0	3.5
4d	0.225 8	0.41	0.22	0.068	0.19	3.5
4f	0.453 1	0.01	0.043	0.0016	0.003	2.0

[a] Observed.
[b] From Ref. 4.
[c] From Ref. 8.
[d] From the calculated cross sections given in Table VI, by normalization to the cross sections for the 4s level. R_d is for excitation from the ground state of neutral He, R_{He^+} is for excitation from the ion ground state, and $R_{He^{++}}$ is for double ionization and subsequent recombination.

show a small axial "drift shift," discussed in Sec. VI, owing to a residual electric field within the discharge which links the microscopic calculations with the variation of the discharge conditons.

IV. GENERAL FEATURES OF DISCHARGE

For a hollow-cathode typically 10 mm in diam and 25 mm long, operated at pressures between 0.05 and 1.5 Torr, and currents 1–40 mA, a bright well-defined glow discharge is formed within the hollow cathode. The discharge boundaries are more diffuse at higher temperatures (77–290 °K) because of the higher random atom velocities preventing the formation of a sharp potential boundary, and allowing motion of the decaying atoms outside the discharge region.

Probe measurements[9–11] have shown that most of the potential fall between cathode and anode in such discharges occurs in the cathode dark space (see Fig. 6). The potential fall within the discharge can be less than 1 V, and a potential fall proportional to the separation of the anode and cathode exists between the discharge and the anode. This separation is made very small, about 2 mm, to minimize the discharge input power.

The anode-cathode voltage $V_t(I)$ increases slowly with the current I, the variations being similar for every cathode material; e.g., for copper, $V_t(0)=200$ V, $V_t(30\text{ mA})=250$ V. These values decrease on cooling to liquid-helium temperatures. On decreasing the pressure or the current, the diameter of the cathode glow shrinks to a minimum diameter of about 0.5 times the cathode diameter. This is consistent with other experiments[11] which show the cathode dark space to be about 5 electron mean free paths. As a result, larger diameter cathodes maintain a discharge at lower pressures, the voltages obeying the following empirical relationship:

$$V_t(I,p,d)=V_0(d)+k(d)I/p\ ,$$

where $k(d)$ is a constant for a cathode diameter d(4–20 mm), and pressure p(0.1–1.5) Torr. The minimum pressure, p_{min}, is proportional to $1/d$, and $V_{t,\,min}$ is approximately independent of d. For $d=10$ mm, $p_{min}\sim 0.5$ Torr at liquid N_2 temperature.

Thus, the hollow-cathode glow forms a relatively field-free region of low-density plasma. Known characteristics of the room-temperature plasma are an electron-ion density of $n_e=n_i=10^{12}$ cm^{-3} within a neutral atom density $n_0=10^{15}$–10^{16} cm^{-3}. In helium, the electron temperature has been measured to be approximately 8 eV in the positive column and about 2 eV in the cathode glow.[12] The neutral atom temperature, measured from the Doppler linewidths of the neutral atoms (see Table III and Fig. 7), tends to be close to the cathode surface temperature, which is much less than that of the electrons. Maintaining this nonthermal equilibrium is the input of the emitted cathode electrons, with energies of 150–200 V. We estimate from the

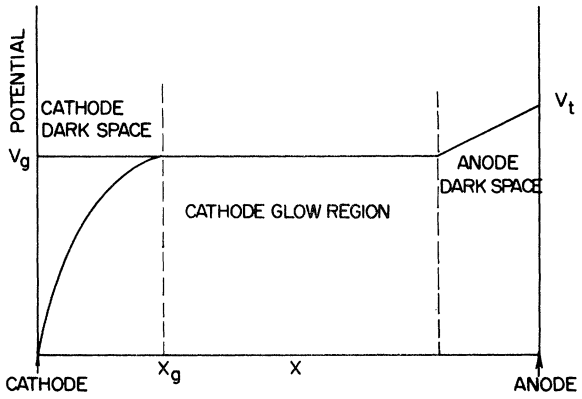

FIG. 6. Representation of the potentials within a hollow cathode. In the type used, the anode-cathode separation was small enough (0.2 cm) to ensure that most of the voltage drop occurred between the cathode and the nearly field-free "glow" region.

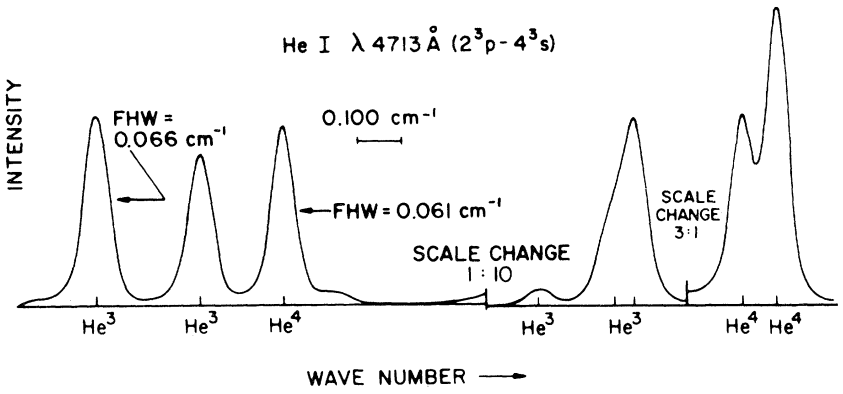

FIG. 7. The He I λ4713 Å $2p\ ^3P_{0,1,2}$-$4s\ ^3S_1$ transition excited in a liquid-helium-cooled aluminum hollow cathode, observed with a two-etalon spectrometer. The helium was a mixture of the two isotopes ^{3}He and ^{4}He. Some of the theoretical positions and experimental full half-widths (FHW) are shown.

various cross sections that these energetic electrons become isotropic in direction by elastic collisions before producing the excited ions, which then decay showing the abnormally high linewidths. The isotropy was verified experimentally by viewing spectra from different directions (0°, 180°, 90°, 45°, and 135°) with respect to the anode-cathode axis: The same mean positions, linewidths, and profiles were observed in each direction.

V. EXCITATION OF He^+ $(n=4,l)$ STATES

Analysis of the atomic-collision processes involved in the excitation and decay of the λ4686 Å He II radiation explains the large width, unusual profile, and anomalous intensities of this line. We consider three possible excitation modes of the He^{+*} $(n=4, l)$ state.

We first consider direct excitation from the neutral ground state:

$$He + e \rightarrow He^{+*}(n=4, l) + e + e \quad .$$

Lee and Lin[13] have shown this reaction to be the dominant mechanism in their production of this state by electron impact, and it was extensively investigated as the most likely method of excitation in the hollow cathode. The total cross section Q_d for this direct process was calculated in several ways. The Born approximation with both a hydrogenic ground-state wave function and also with a more accurate ground-state wave function agreed to within 10%. Two variants of the Gryzinski[14] classical model for two-body impact, differing in treatment of the third electron and the nucleus, also agreed to within a factor of 2. The probability $I_l(P)$ of excitation to the ionized (n, l) state with final momentum P calculated using the Born approximation is

$$I(P) = \int_0^{\pi} d\Theta \int_{k_3(\min)}^{k_3(\max)} dk_3 I_{k_3}(l) J(\Theta, k_3) \quad ,$$

where Θ is the recoil angle of the ion, k_3 the wave vector of the ejected electron, and J and I_{k_3} are given in the Appendix along with other details of the calculation. The integrations have to be completed numerically. $I(P)$ is shown for $l=0$ in Fig. 8. The full half-widths of the momentum transfer-line profile $L(p) = (1/p^2)I(p)$ for the different $n=4, l$ states are given in Table V for three different incident electron energies.

To obtain the theoretical line profile for the hollow cathode, we must combine this momentum-transfer velocity with the random thermal velocity of the colliding atom, which for these experiments

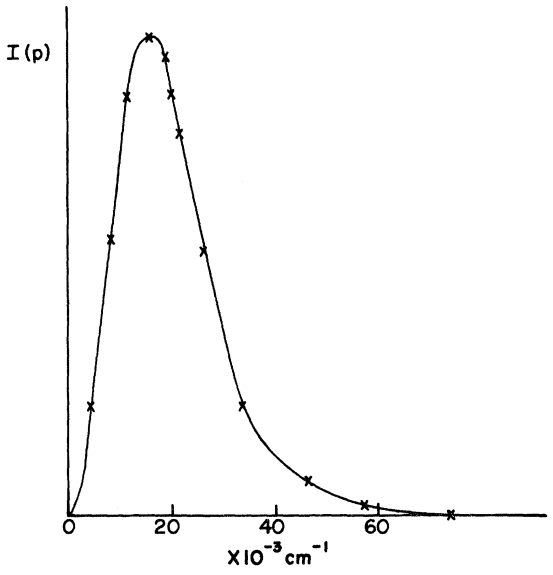

FIG. 8. Momentum-transfer profile for the $n=4$, $l=0$ He^+ state excited by 200-eV electrons. The momentum scale is converted to the equivalent Doppler shift for the λ4686 Å line of the isotope ^{4}He. The scale for the isotope ^{3}He would be $\frac{4}{3}$ times this scale. The resultant profiles for the $l=1, 2, 3$, states of $n=4$ have different widths, but a similar shape. Half-widths of the resultant line profiles are given in Table V. The points actually calculated are indicated.

TABLE V. Calculated half-widths of the momentum-transfer line profile for the components of the 4686 Å line of He^+, expressed in 10^{-3} cm^{-1}.

Electron kinetic energy, eV	Full half-widths [a] for ^4He			
	4s	4p	4d	4f
250	27	41	41	41
200	27	43	43	44
150	26	46	45	45

[a]These widths multiplied by $\frac{4}{3}$ are appropriate for ^3He.

was similar in magnitude. If p_1, $I(p_1)$ and p_2, $M(p_2)$ denote the momenta and isotropic distribution function for excitation and thermal motion, respectively, then the probability of final momentum p is given by

$$F(p) = \int_0^\infty dp_1 \int_{|p-p_1|}^{p+p_1} dp_2 \, (p/p_1 p_2) I(p_1) M(p_2) ,$$

and the line profile becomes $L(p) = (1/p^2)F(p)$.

The momentum transfer to the ion in this process is found to be greater than that transferred in the electronic excitation of neutral helium states. For neutral ^4He, full half-widths of about 0.010 cm^{-1} are obtained for allowed electric dipole transitions to P states, and widths up to 0.035 cm^{-1} are obtained for excitation to S states.[15] The momentum-transfer profiles for excitation to the $He^+(4l)$ states (Fig. 8) are very close to Maxwell-Boltzmann distributions. Using two such distributions in the above integral equation, one for the momentum transfer and one for the thermal distribution determined from He I lines, yields half-widths of 63×10^{-3} cm^{-1} for the ^4He 4p, d, f states. Although this is 0.015–0.020 cm^{-1} smaller than the experimental results, it is well within the calculational accuracy and is considered as explaining the observed widths. The 4s-state calculation produces a smaller half-width, whereas observed widths are roughly 10% larger. The large 4s width must, nevertheless, be due to the excitation process, since the same increase is also seen in the electronic excitation of this state in the collisionless neutral helium beam.[8] However, the accuracy of these calculations is not very great, and a factor-of-2 variation is easily possible.

Larson and Stanley find that the atomic-beam-produced line profiles are predominantly Gaussian, in agreement with the above theory. In the hollow cathode, however, the profiles show an extended wing. This wing shows on traces taken with the PEPSIOS, on which extremely high instrumental contrast is achieved, and with the WBS, but does not show on traces of He I lines. Consequently, it cannot be instrumental in origin, and very likely arises from the excitation of ions (see below) which have been heated either by the rather strong fields which surround the hollow-cathode plasma or by excitation processes involving greater momentum transfer.

If the momentum-transfer process is the principal cause of the excessive linewidths, then the linewidth ratio for the two isotopes should be the inverse of the mass ratio ($m_4/m_3 = 1.33$). An energy process, i.e., an equilibrium in temperature, would produce a linewidth ratio equal to $(m_4/m_3)^{1/2} = 1.15$, and perturbations by magnetic or electric fields would produce a mass-independent width. Table III shows a width ratio of 1.21 after deconvolution to remove the instrumental profile. If we then deconvolute a Gaussian half-width corresponding to the temperature derived from the neutral helium linewidths (see Fig. 7), the ratio of the remaining linewidth is 1.30, very close to that expected for a momentum-transfer process.

We have observed similar anomalously large widths in other ionized helium transitions: λ3203 Å $n = 5 \rightarrow 3$; λ10124 Å $n = 5 \rightarrow 4$; λ6560 Å $n = 6 \rightarrow 4$; λ5411 Å $n = 7 \rightarrow 4$; and λ4860 Å $n = 8 \rightarrow 4$. The detailed analysis has not been carried out for these other lines.

The second excitation process considered is electronic excitation from the ion ground state:

$$He^+(1s\,^2S_{1/2}) + e \rightarrow He^+(n = 4, l) + e .$$

The cross section Q_i for this process was calculated by scaling the results for the equivalent reaction in hydrogen, ignoring the effects of the long-range Coulomb field of the He^+ ion. Comparing the results for electronic excitation of H and He^+ [16] indicates that this assumption is valid. To find the importance of the above reaction, the population of the He^+ ground state must be known. If R is the ionization ratio in the plasma, then RQ_i should be compared with the direct-process cross section Q_d (see Table VI, where $R = 10^{-4}$).

This process will enhance the population of the 4p states. The momentum transfer is expected to be less than for the direct process, but the initial velocities of the ions will be different. Ion veloc-

TABLE VI. Calculated cross sections for excitation of the $n = 4$ levels of He^+. [a]

Upper level	4s	4p	4d	4f
Q_d	8.1	2.9	0.68	0.01
$Q_i \times 10^{-4}$ [b]	0.3	3.0	0.05	0.0007
Q^{++}	0.22	0.77	0.77	0.44

[a]Units are 10^{-21} cm^2.

[b]Cross sections for excitation from the ion ground state have been multiplied by 10^{-4}, the estimated ionization ratio in the hollow cathode, for comparison with the cross section Q_d for the direct ionization-excitation process from the ground state of neutral He.

ities are expected to be greater than the neutral velocities because the smaller ion diameter makes collisions with neutrals less likely and because the ions are more efficiently heated through the Coulomb interaction with the electrons. Thus, the width of lines excited by this process may not be very different from widths observed in the neutral excitation process. (Note also that a group of ions of much higher velocities is suggested by the extended wing of the line profile mentioned above.)

The third process is electron excitation to the doubly ionized helium ion

$$\mathrm{He} + e \rightarrow \mathrm{He}^{++} + e + e + e \ ,$$

with subsequent cascading, after a single-electron recombination, through the $\mathrm{He}^{+*}(n=4,l)$ states. The cross section for electronic double excitation has been measured experimentally[17] and calculated in the Born approximation,[18] and it is found that $\sigma^{++} \approx \sigma^{+}/200$.

The He^{++} may decay by two processes. First, it recombines with an electron into an exicted He^{+} state and cascades down to the He^{+} ground state

$$e + \mathrm{He}^{++} \rightarrow \mathrm{He}^{+*}(n) \rightarrow \mathrm{He}^{+}(1s\ ^2S_{1/2}) \ .$$

Of the $n=4$ states, this process will tend to populate the states of higher angular momentum. The recombination rate directly to the $n=4$ states is the most important, the cascading from the highest n states giving a small increase in the $4f$ states.

The competing process is charge exchange with a neutral atom:

$$\mathrm{He}^{++} + \mathrm{He}(1s\ ^1S_0) \rightarrow \mathrm{He}^{+}(n,l) + \mathrm{He}^{+}(n',l') \ .$$

There is only sufficient energy available to leave both ions in the ground state, and thus this process deexcites the He^{++} with no 4686 Å radiation. Using a semiempirical method,[19] the charge exchange cross section is calculated to be

$$Q_{\mathrm{ex}} = 4 \times 10^{-19}\ \mathrm{cm}^2 \ .$$

The recombination cross section Q_R for He^{++} was assumed to be Z^2 times that for hydrogen.[20] The fraction f_l of recombinations producing ions in the state $\mathrm{He}^{+*}(n,l)$ is

$$f_l = Q_R(n,l)/Q_{\mathrm{tot}} \ ,$$

where Q_{tot} is the cross section for all decays:

$$Q_{\mathrm{tot}} = \sum_{n,l} Q_R(n,l) + (N_0/N_e)(v_0/v_e)Q_{\mathrm{ex}} \ ,$$

where N_0, v_0 and N_e, v_e are the number density and velocity of the neutral atoms and electrons, respectively. The resultant cross section to the $\mathrm{He}^{+*}(n=4,l)$ state through the double ion is $Q^{++} = \sigma^{++} f_l$, and is compared with the cross sections for other excitation processes in Table VI.

The observed relative excitation rates were given in Table IV, which also gives calculated relative rates for the processes discussed above. The low $4p$-state population relative to the $4s$-state population for both the hollow cathode and the atomic beam indicates that the direct process of excitation is much more likely than excitation through the ion ground state. A close-coupling calculation[21] on the excitation of $\mathrm{He}^{+}(2s,2p)$ from $\mathrm{He}^{+}(1s)$, and also the similar excitations to the $\mathrm{He}(1s,3l$ and $4l)$ states from the $\mathrm{He}(1s^2)$, gives cross sections favoring the p states over the s states by a factor of about 15.[22] Then the relative cross sections Q_i, which give a ratio $Q_i(4p)/Q_i(4s) = 12$, are expected to be quite reliable. Thus, the two-step process through the ion ground state can account for the $4p$-state population while having very little effect on the other $n=4$ states. However, the calculation of the $4p$, d, f rates in the direct process may be off by a factor as large as 5 because under the Born approximation these cross sections are governed by the overlap integral between the $1s$ electron and the ionized electron. This is very sensitive to the choice of the effective charge in the wave function of the ionized electron.[13] Furthermore, the cross section for direct excitation of the $4f$ state may be much larger than the value obtained by the Born approximation because of the close coupling between the $4p$, $4d$, and $4f$ states.[23] The values obtained for Q^{++} show that recombination might account for the high population of the $4d$ and $4f$ states. Increasing the cathode current at a fixed pressure increases the relative populations of the $4p$ states in agreement with the increased ionization ratio R. More refined calculations of the direct mechanism are needed to more precisely determine the relative importance of the various processes.

Larson and Stanley[8] observed this transition produced by crossed beams of 500-V electrons and neutral helium atoms. Their excitation widths were comparable ($\approx 0.085\ \mathrm{cm}^{-1}$) to those of the hollow cathode ($0.080\ \mathrm{cm}^{-1}$) and much wider than the observed neutral widths. This confirms that the width arises in the excitation process, since the atomic-beam density is low enough to rule out any collision during decay. Table III compares the widths seen. We conclude that the excitation processes are basically the same for the beam and the hollow cathode, and that small differences in width, profile, and relative intensities come partially from collisions during deexcitation in the cathode (discussed below), and partially from differences in the initial neutral atom-, ion-, and electron-velocity distributions.

VI. DEEXCITATION OF $He^{+*}(n=4,l)$ STATES

For gas densities encountered in the hollow cathode, collisions of the excited helium ions with neutral atoms and electrons must be considered. Collisions with other ions may be neglected because of the low ionization ratio and the low ion velocity. Although the major excitation processes in both the atomic beam and the hollow cathode appear to be the same, the relative intensities in the hollow cathode are altered by collisions which deexcite or redistribute the population of the upper excited states. Variations in the relative intensities of the components observed in a hollow cathode have been previously studied.[4] We consider here some details of the deexcitation mechanisms.

Ion-electron collisions are dominated by the Coulomb force. For electrons of velocity v_0 and helium ions, the impact parameter for an electron scattered through an angle θ is $b=(Ze^2/mv_0^2)\cot\frac{1}{2}\theta$, and the momentum transfer to the ion is $P=MV=2mv_0\sin\frac{1}{2}\theta$. For $Z=1$ and 1-eV electrons, $b=0.8\times10^{-7}\cot\frac{1}{2}\theta$. Taking $v_0=6\times10^7$ cm sec^{-1} and $n_e=10^{12}$ cm^{-3} gives a reaction rate $R=b^2n_ev_0=1.0\times10^6\cot^2(\frac{1}{2}\theta)$. Thus, a significant number of collisions will occur within the lifetime of the excited states (3×10^{-9} sec) only for $\cot^2(\frac{1}{2}\theta)>100$ or $\sin\frac{1}{2}\theta>0.1$, for which the momentum transfer is negligible. We conclude that there would be very little heating effect due to ion-electron collisions; however, this Coulomb interaction may cause inelastic collisions which redistribute the populations in the different $n=4$, l states, tending toward the statistical distribution. Assuming that the energy transferred to the ion in scattering is similar to that needed to make changes among the $n=4$ sublevels, we find the angle of scattering required is $\theta\approx0.06$ rad, giving a collision time $\tau_i=5\times10^{-8}$ sec, which is too high to be appreciable for all except the 4s states. Moreover, we have certainly overestimated the collision cross section for this process. However, at higher cathode currents we may be seeing such an effect in the slight broadening of the lines, and also in the approach to statistical distributions, particularly through redistribution of the more highly populated 4s levels. Similar collisions with the ions could give larger momentum transfer, but are reduced in probability by a factor of 100 through the lower ion velocity. The non-Coulomb forces have a cross section $<10^{-14}$ cm^2 with a collision time of $\tau_i>3\times10^{-7}$ sec, which is too long to be important.

The elastic-collision frequency with neutral atoms in the hard-sphere approximation is found using mean radii calculated[24] from the wave functions for the different $n=4,l$ states and the ground state of neutral He.[25] The relative velocity is essentially that of the ions, and for a pressure of 0.5 Torr at liquid-helium temperature, we obtain an average collision rate $R=1.5\times10^8$ sec^{-1} and a collision time $\tau_i=6.7\times10^{-9}$ sec. This is of the same order of magnitude as the natural decay lifetimes. The rapid variations with pressure observed in the relative intensities of the components,[4] together with consideration of the various collision times, lead to the conclusion that collisions of excited ions with neutral atoms are primarily responsible for the deexcitation and population redistribution in the $n=4$ levels. Measurements of the drift shift substantiate our conclusions.

VII. ANODE DRIFT SHIFT

The anode drift shift is the Doppler shift in wave number of the fine structure components of $\lambda4686$ Å on observing the hollow cathode in the two directions, 0° and 180°, to the anode-cathode axis. It is positive when the shift implies a motion of the ion away from the anode, i.e., a violet shift when the anode is furthest from the observer.

A small residual electric field within the hollow-cathode discharge was postulated by Roesler and De Noyer.[26] This field accelerates the ions away from the anode during their decay. The neutral atom should be unaffected, and the measurements of the He I line λ 4713 Å ($4^3S_1\rightarrow2^3P_{0,1,2}$) showed drift shifts of less than the experimental limit of ±0.0005 cm^{-1}, verifying both the zero drift shift and the absence of any significant instrumental shift on switching the anodes. Thus, the drift shift is postulated to be a measure of the ion velocity gained by acceleration in this field while radiating.

Consider first the case in which the ion radiates before undergoing any type of collision. If E is the electric field, M the mass of ion, and τ_l the time for the $n=4$, l state to radiate, then the drift velocity is

$$v_d=(Ee/M)\tau_l\,.$$

If the ion undergoes collisions before radiating, the drift velocity is determined by the collision time $\tau_{c,l}$ for each l state:

$$v_{c,l}=(Ee/M)\tau_{c,l}\,,$$

where $\tau_{c,l}=1/N\sigma_lV_l$, N being the density of the colliding particles, σ_l the collisional cross section, and V_l the relative velocity.

As seen above, the neutral collisions are most probable. The neutral atom density is $N=P/kT$. The relative velocity V_l is approximately the ion velocity, since this, from linewidth measurements, appears much larger than the neutral atom velocity. The cross section is $\sigma=\pi(r_l+r_0)^2$, where r_l is the radius of the excited ion and r_0 the radius of the neutral atom. Thus,

$$v_c = (T/P)Ee(1/MV_l)1/\pi(r_l + r_0)^2 .$$

Figure 9 shows how the drift shifts vary with pressure for the two separated isotopes. It should be noted that:

(i) The shift for component 4(4p) (the n, l values for the upper state of each component are given in parentheses) is always close to zero, and sometimes negative. This agrees with its short lifetime, not having time to accelerate in the field before radiating.

(ii) Component 1(4d) has a small positive shift, decreasing slowly as the pressure increases. Assuming it to be accelerated over its decay lifetime, we can obtain a value for the electric field within the plasma. For a typical 4d shift of 0.006 cm^{-1}, we obtain a field within the discharge of 1.5 V/cm. The decrease of the 4d shift with increasing pressure is explained by a decrease of the electric field. As the pressure increases, the edges of the plasma move closer to the cathode wall giving a larger volume of stable plasma, reducing its internal electric field.

(iii) Components 5(4d + 5f), 9(4f), 3(4s), and 12(4s) have shifts decreasing rapidly with pressure. Both the increase of collisions and the reduction in the electric field contribute to this decrease. The 4f shift is greater than the 4s shift, corresponding to the smaller diameter of the 4f state. The 4d contribution to the shift in component 5 reduces it below that of component 9.

(iv) The isotope dependence shows that the ^{3}He shifts are slightly larger than the ^{4}He shifts. This is expected especially for the 4d states which decay without collisions. The residual electric-field dependence on isotope mass is uncertain; however, drift-shift measurements in mixed isotopes also show larger ^{3}He shifts.

(v) The larger diameter cathodes (see Fig. 10) give rise to a smaller axial electric field (zero for diameters above $\frac{5}{8}$ in. in the larger plasma, and hence smaller drift shifts.

For a given cathode we can fit the above drift shifts to formulas: (i) $\Delta\sigma = k_1[E(p)/M]\tau_l + \alpha_1$ for the collisionless 4p and 4d transitions; (ii) $\Delta\sigma = k_2[E(p)/p](1/\sigma_l) + \alpha_1$ for the collision limited 4s, 4d, and 4f states; k_1 and k_2 are numerical constants, and α_1 is a measure of the bulk ion velocity immediately after being excited. This is seen in the drift shift of the 4p decays which are very rapid.

The anode drift shift confirms the calculations that during decay of the $He^{+*}(n=4)$ states collisions with the neutral atoms are more likely than electron collisions. It also indicates that these collision rates are of the same order as the natural lifetimes of the different states resulting in a small number of collisions for the longer-lived states. This produces a net cooling of the excited states during decay, which does not occur for the "collisionless" helium atomic beam, and may in part account for the smaller linewidths observed from the hollow cathode (Table III).

VIII. CONCLUSION

This high-resolution study of the fine structure of the He II λ4686 Å $n = 3-4$ complex has explained the origin of the intensity and half-width anomalies

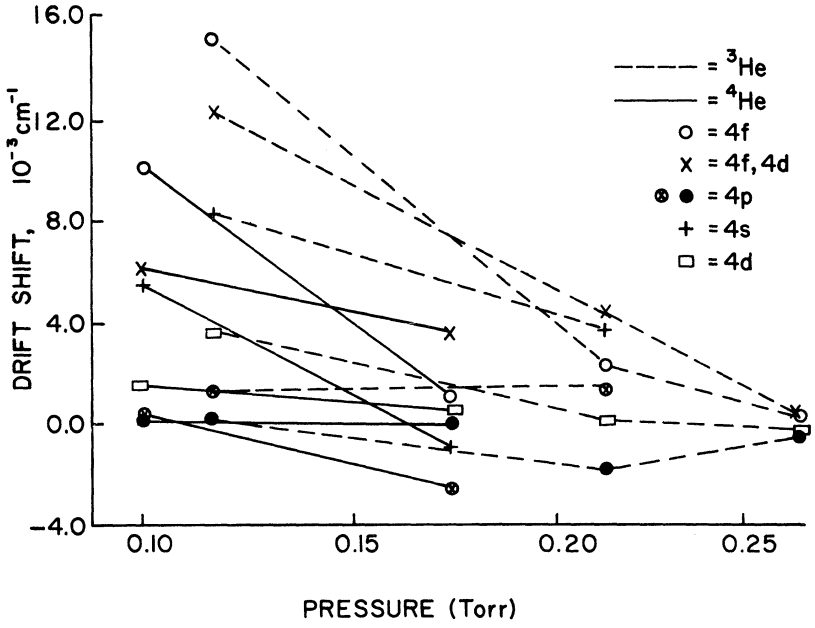

FIG. 9. Drift shift for each isotope as a function of pressure for a liquid-helium-cooled aluminum hollow cathode, 0.12 cm in diam. The n, l values for the upper state of each transition are shown.

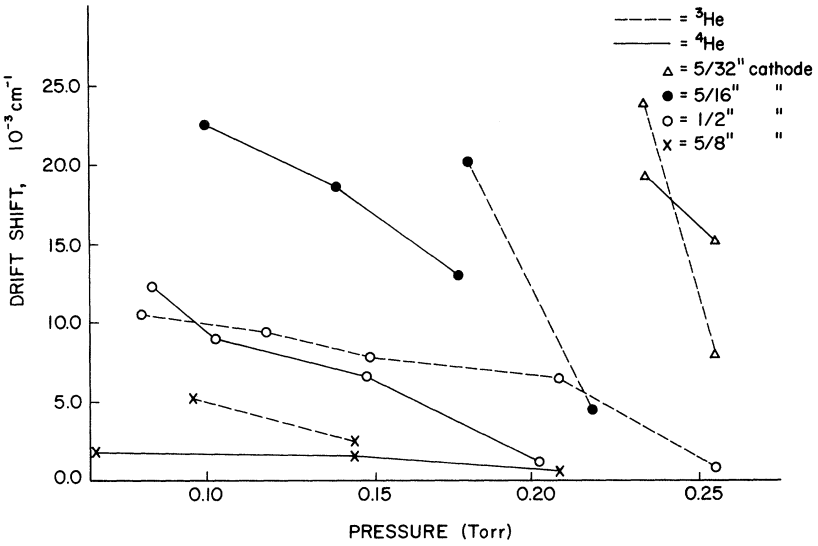

FIG. 10. Variation in drift shift with hollow-cathode diameter. The results are of qualitative significance only, because of uncertainties in the exact pressure at which each cathode was operated.

in terms of the discharge mechanisms which themselves can now be more fully understood. In particular, the anomalous widths observed in the atomic beam as well as in the hollow cathode have been explained as a momentum-transfer process. This momentum-transfer width appears to be a physical limit to the attempts during the previous 50 yrs to produce narrow spectral-line sources by electronic excitation. It has been confirmed that the relative shift in wave number (drift shift) of the transitions from different angular momentum substates arises from a small axial electric field in the plasma. After correcting for the drift shift, fine structure and isotope shift measurements agree with quantum electrodynamics.

ACKNOWLEDGMENTS

The authors wish to acknowledge with thanks many helpful discussions with C. C. Lin on the excitation processes. H. P. Larson and R. W. Stanley of Purdue University are thanked for the use of their helium atomic-beam results.

APPENDIX: DIRECT CROSS SECTION

We calculated the momentum transfer to the excited ion in the process

$$\mathrm{He}+e\rightarrow \mathrm{He}^{+*}(n=4,l)+e+e \ .$$

The differential cross section of Lee and Lin[13] is

$$Q_{k_3}\,d\sigma\,d\omega\,dk_3=\frac{k_2}{4\pi^2k_1}\left|\int V\Psi_i\Psi_f^{*}e^{i\vec{K}\cdot\vec{r}}\,d\tau_1\,d\tau_2\,d\tau\right|^2 d\sigma\,d\omega\,dk_3 \ ,$$

where

$$V=\frac{1}{\vec{r}-\vec{r}_1}+\frac{1}{|\vec{r}-\vec{r}_2|}-\frac{2}{r} \ ,$$

the momenta are as shown in Fig. 11, and the wave functions are screened hydrogenic wave functions. The incident electron has been scattered into the solid angle $d\sigma$ and the ejected electron into the solid angle $d\omega$. Then, integrating Q_{k_3} over $d\sigma, d\omega$, and dk_3, we obtain the cross section for a momentum transfer $\vec{P}$ to the ion.

$$I_l(p)=\int_0^{\pi}d\Theta\int_{k_3(\min)}^{k_3(\max)}I_{k_3}(l)J(\Theta,k_3)dk_3 \ ,$$

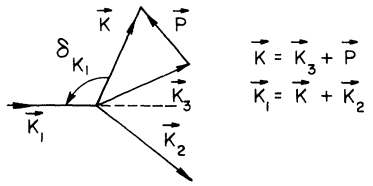

FIG. 11. Wave vectors for the direct excitation to the He^{++} (n,l) state; $\vec{k}_1$ and $\vec{k}_2$ are those of the incident and scattered electron, $\vec{k}_3$ the wave vector of the ejected electron, and $\vec{P}$ that for the excited ion.

where

$$J(\Theta, k_3) = \sin\Theta[k_3^2 - P^2\sin^2\Theta]^{-1/2} ,$$

$$\cos\alpha = (1/k_3)\{k_3^2 - P^2\sin^2\Theta]^{1/2} ,$$

$$K = P\cos\Theta + [k_3^2 - P^2\sin^2\Theta]^{1/2} ,$$

$$l = 0, \quad I_{k_3}(0) = \frac{2^6\mu^6\pi k_3}{k_1^2 K} \frac{(P^2 - k_3^2 + (K^2+\mu^2)\cos^2\alpha)}{(p^2+\mu^2)^4[(\mu^2+K^2-k_3^2)^2 + 4\mu^2 k_3^2]}$$

$$\times \frac{1}{1-\exp(-2\pi\mu/k_3)} \exp\left[-\frac{2\mu}{k_3}\arctan\left(\frac{2\mu k_3}{K^2+\mu^2-k_3^2}\right)\right] ,$$

$$l \neq 0, \quad I_{k_3}(l) = \frac{2^5\pi^5\alpha^2 e^4}{k_1^2 K^8}\left(\frac{na_0}{2Z'}\right)^2 \frac{(n-l-1)!(2l+1)!}{(n+l)!^3} |I_{n,l}|^2$$

$$\times 2^6\pi\mu^2 \frac{(1-\epsilon')^2\epsilon'}{k_3(\mu^2+k_3^2)^4} \frac{1}{1-\exp(-2\pi\mu\epsilon'/k_3)} \exp\left[-\frac{2\mu\epsilon'}{k_3}\tan^{-1}\left(\frac{2\mu k_3}{k_3^2-\mu^2}\right)\right] .$$

$I_{n,l}$ are the Gegenbauer polynomials:

$$I_{4,3} = 3D, \quad I_{4,2} = 2Dx(12/q - 1), \quad I_{4,1} = 3D[(3/q^2)(7x^2-1) - 4x/q + 1],$$

$$D = \frac{2^{l+5/2}(2l+2)!\zeta^{l+1/2}}{\Gamma(l+\frac{3}{2})[(\epsilon+n)^2+\zeta^2]^{l+2}}, \qquad q^2 = \frac{(n-1)^2+4\zeta^2}{(\epsilon+n)^2+4\zeta^2} ,$$

$$x = \frac{1}{q}\frac{(\epsilon+n)(n-1)+4\zeta^2}{(\epsilon+n)^2+4\zeta^2}, \quad \epsilon = Z/Z', \quad \epsilon' = Z/Z'', \quad \zeta = K(na_0/2Z') .$$

Z' is the shielded nuclear charge of the helium ground state, $=1.69$. Z'' is the shielded nuclear charge seen by the outgoing electron, and is tabulated in Ref. 13:

$$l = 1, \ Z'' = 1.45; \quad l = 2, \ Z'' = 1.53; \quad l = 3, Z'' = 1.5 .$$

The authors are indebted to E. T. P. Lee and C. C. Lin for carrying out the above integration on the computer at the University of Oklahoma, Norman, Okla., to produce the momentum-transfer profile shown in Fig. 8.

[1]J. E. Mack and N. Austern, Phys. Rev. 72, 972 (1947).

[2]G. W. Series, Proc. Roy. Soc. (London) A226, 377 (1954).

[3]G. Herzberg, Z. Physik. 146, 269 (1956).
[4]F. L. Roesler and J. E. Mack, Phys. Rev. 135, 58 (1964).
[5]J. E. Mack, D. P. McNutt, F. L. Roesler, and R. Chabbal, Appl. Opt. 2, 873 (1963).
[6]H. G. Berry (unpublished).
[7]J. D. Garcia and J. E. Mack, J. Opt. Soc. Am. 55, 845 (1965).
[8]H. P. Larson and R. W. Stanley, J. Opt. Soc. Am. 57, 1439 (1967).
[9]H. Schuler, Z. Physik 35, 323 (1926).
[10]W. Kreye (private communication).
[11]F. Llewelyn-Jones, The Glow Discharge and Introduction to Plasma Physics (Methuen and Co. Ltd., London, 1966).
[12]V. S. Borodin and Yu. M. Kagan, Zh. Tekhn. Fiz., (1966) [English transl.: Soviet Phys. – Tech. Phys. 11, 131 (1966)].
[13]E. T. P. Lee and C. C. Lin, Phys. Rev. A138, 302 (1965).
[14]M. Gryzinski, Phys. Rev. 115, 374 (1959).
[15]F. A. Forolyov and V. I. Odintsov, Opt. i Spektroskopiya 18, 968 (1965) [Opt. Spectry. (USSR) 18, 547 (1965)].
[16]A. Burgess and M. R. H. Rudge, Proc. Roy. Soc. (London) A273, 372 (1963).
[17]D. D. Briglia and D. Rapp, Bull. Am. Phys. Soc. 11, 69 (1966).
[18]Margaret J. Fulton and M. H. Mittleman, Phys. Rev. A138, 667 (1965).
[19]N. F. Mott and H. S. W. Massey, The Theory of Atomic Collisions (Clarendon Press, Oxford, 1965), 3rd ed., p. 659ff.
[20]C. W. Allen, Astrophysical Quantities (Athlone Press, London, 1955).
[21]P. G. Burke, D. D. McVier, and K. Smith, Proc. Phys. Soc. (London) 83, 397 (1964).
[22]R. M. St. John, F. L. Miller, and C. C. Lin, Phys. Rev. 134, A888 (1964).
[23]S. Chang and C. C. Lin, Bull. Am. Phys. Soc. 13, 214 (1968).
[24]E. U. Condon and G. H. Shortley, Theory of Atomic Spectra (Cambridge University Press, New York, 1953), 2nd ed., p. 117.
[25]C. L. Pekeris, Phys. Rev. 115, 1216 (1959).
[26]F. L. Roesler and L. De Noyer, Phys. Rev. Letters 12, 396 (1964).

PHYSICAL REVIEW A VOLUME 1, NUMBER 5 MAY 1970

Low-Temperature Mobility of the Electron Bubble in Dilute He^3-He^4 Mixtures and Pure He^3†

Lorenz Kramer*
Institute of Theoretical Physics, Department of Physics, Stanford University, Stanford, California 94305
(Received 30 July 1969)

Recent low-temperature measurements of the mobility of negative ions in dilute He^3-He^4 mixtures are explained. A new method based on the Boltzmann equation is used to derive the general formula for the drag force of a heavy impurity in an arbitrary gas. It is shown that the structure of the negative ion (electron bubble) depends on the He^3 concentration C_3 and temperature. Also, for C_3 above about 1% the distortion of the He^3 distribution by the moving ion becomes important. The application of our theory to pure, highly degenerate He^3 shows that the mobility remains finite at $T=0$ and rises with temperature. Both results agree with experiment.

I. INTRODUCTION

Recently, Meyer and Neeper[1,3] have studied the mobility of positive and negative ions in dilute He^3-He^4 mixtures with atomic He^3 concentration C_3 ranging 1.5×10^{-4} to $4.4.\times10^{-2}$. In their temperature region ($0.05\,^\circ\mathrm{K} \leq T \leq 0.5\,^\circ\mathrm{K}$) the mobility is determined by He^3 scattering except in the very dilute case, where a small correction for phonon scattering is necessary. Some of the experimental results for $\mu_0 C_3$, where μ_0 is the low-field mobility,[3] are shown in Fig. 1. One sees that the product $\mu_0 C_3$ does not depend very much on concentration. The remaining variation of $\mu_0 C_3$ with concentration, its rather complicated temperature dependence, and the vast difference in the behavior of the positive and negative ions impose severe restrictions on a theoretical explanation. We present a theory that explains some of the observed features and yields quite good agreement with the experimental results on negative ions.

For our purposes we assume that the He^3-He^4